The Fate of Sediment After a Large Earthquake

Oliver Richard Francis[1], Xuanmei Fan[2], Tristram Charles Hales[3], Daniel Edward James Hobley[4], qiang xu[2], and Huang Runqui[2]

[1]Helmholtz-Zentrum Potsdam - Deutsches Geoforschungszentrum
[2]Chengdu University of Technology
[3]Cardiff University
[4]University of Colorado Boulder

November 30, 2022

Abstract

Large earthquakes cause rapid denudation of hillslopes by triggering thousands of coseismic landslides. The sediment produced by these landslides is initially mobilised out of the landscape as a cascade of unknown magnitude. This cascade dramatically enhances local erosion rates before rapidly returning to pre-earthquake levels. Identifying the individual processes of this cascade and estimating the volume of sediment they mobilise is crucial to determining the timescales over which earthquakes can influence hazards and sedimentary systems. Here we present a fully constrained sediment budget of the first decade after the 2008 Mw 7.9 Wenchuan earthquake. With this budget we identify the key erosion processes within the post seismic sediment cascade and constrain estimates of the volume of sediment removed from the landscape. With these estimates we find that over 90% of the coseismically generated sediment remaining on the hillslope 10 years after the earthquake. Despite the large volumes of sediment on the hillslope, we observe an order of magnitude decrease in the erosion rate of the epicentral area. Debris flows are the key erosional mechanism of the coseismically generated sediment as erosion rates are correlated with debris flow frequency. Erosion rates likely remain elevated for several decades however, the rapid stabilisation of the sediment following the earthquake suggests large volumes of coseismically generated sediment can remain in orogens for hundreds or thousands of years. In the most tectonically active regions, the long residence times of coseismically generated sediment could significantly reduce bedrock incision rates in channels altering long term erosion rates.

The Fate of Sediment After a Large Earthquake

Oliver Francis[1,2,*], Xuanmei Fan[3], Tristram Hales[1,2], Daniel Hobley[2], Qiang Xu[3], Runqiu Huang[3]

[1]Sustainable Places Research Institute, Cardiff University, Cardiff, United Kingdom

[2]School of Earth and Environmental Sciences, Cardiff University, Cardiff, United Kingdom

[3]State Key Laboratory for Geohazard Prevention and Geoenvironment Protection, Chengdu University of Technology, Chengdu, China

Corresponding author: Oliver Francis (Oliver.Francis@gfz-potsdam.de)

*Now at Section 4.7: Earth Surface Process Modelling, German Research Centre for Geosciences (GFZ), Potsdam, Germany

Key Points:

- Significant volumes of sediment produced by the 2008 M_w7.9 Wenchuan earthquake remain on the hillslope 10 years after the event.
- Debris flows rather than fluvially driven erosion are the key process in transporting sediment from the hillslope into the main river.
- The decrease in debris flows frequency in the decade since 2008 is coincident with an order of magnitude reduction in sediment export.

Abstract

Large earthquakes cause rapid denudation of hillslopes by triggering thousands of coseismic landslides. The sediment produced by these landslides is initially mobilised out of the landscape as a cascade of unknown magnitude. This cascade dramatically enhances local erosion rates before rapidly returning to pre-earthquake levels. Identifying the individual processes of this cascade and estimating the volume of sediment they mobilise is crucial to determining the timescales over which earthquakes can influence hazards and sedimentary systems. Here we present a fully constrained sediment budget of the first decade after the 2008 M_w7.9 Wenchuan earthquake. With this budget we identify the key erosion processes within the post seismic sediment cascade and constrain estimates of the volume of sediment removed from the landscape. With these estimates we find that over 90% of the coseismically generated sediment remaining on the hillslope 10 years after the earthquake. Despite the large volumes of sediment on the hillslope, we observe an order of magnitude decrease in the erosion rate of the epicentral area. Debris flows are the key erosional mechanism of the coseismically generated sediment as erosion rates are correlated with debris flow frequency. Erosion rates likely remain elevated for several decades however, the rapid stabilisation of the sediment following the earthquake suggests large volumes of coseismically generated sediment can remain in orogens for hundreds or thousands of years. In the most tectonically active regions, the long residence times of coseismically generated sediment could significantly reduce bedrock incision rates in channels altering long term erosion rates.

Plain Language Summary

Earthquakes produce large volumes of sediment by triggering landslides in mountain ranges. Immediately after an earthquake there is an order of magnitude increase in erosion rates, however this period of enhanced erosion is short lived. Understanding the mechanisms which control the timespan of the elevated erosion rates and the rates at which they move sediment is vital for determining the continuing impact the earthquake has on the landscape. Using satellite imagery to map and track the movement of sediment after the 2008 Wenchuan earthquake we show that more than 90% of the sediment produced by the earthquake remains on the hillslope a decade after the earthquake. Debris flows initiating in the landslide deposits are responsible for most of the erosion during this time. The frequency of these flows decreases rapidly after the earthquake reducing the overall erosion rates close to normal levels. The remaining sediment could reside in the orogen for hundreds or thousands of years indicating that it could have a significant impact on long term erosion rates and landscape evolution.

1 Introduction

Large, continental earthquakes can produce thousands of coseismic landslides mobilising several cubic kilometres of sediment from the hillslope (Keefer 2002; Malamud et al. 2004). Coseismic landsliding is likely to be a key erosional process in these regions, potentially accounting for over 50% of long term erosion rates (Li et al. 2014; Marc et al. 2016b; Marc et al. 2016a; Li et al. 2017). Understanding how earthquakes affect the evolution of landscapes requires a consideration of both the direct impact of the landslides on hillslopes and how the erosion or storage of the sediment impacts the evolution of the channel network (Egholm et al. 2013; Campforts et al. 2020). Coseismic landslides reduce the relief of steep hillslopes and can alter the size of drainage basins via erosion of basin ridges (Schmidt and Montgomery 1995; Dahlquist et al. 2018). While the landslide deposits contribute to debris flow generation (Fan et al. 2019b) and provide tools or cover for abrading/protecting the bedrock channels (Turowski and Rickenmann 2009; Yanites et al. 2010; Egholm et al. 2013) altering the evolution of upland rivers. Long term storage of the coseismically generated sediment can dampen the isostatic response of an earthquake (Densmore et al. 2012) or reduce the bedrock erosion of future earthquakes (Li et al. 2014; Marc et al. 2016b; Stolle et al. 2019; Francis et al. 2020). Therefore, to fully incorporate earthquakes into models of long-term landscape we must understand the processes and timescales by which coseismically generated sediment is exported from orogens. Key to this aim is fully understanding and quantifying the erosional processes of the coseismically generated processes following earthquakes.

Following large earthquakes it is typical (though not always (Tolorza et al. 2019)) to see an order of magnitude increase in sediment discharge in orogen draining rivers (Pain and Bowler 1973; Hovius et al. 2000; Dadson et al. 2004; Hovius et al. 2011; Wang et al. 2015). However, this period of elevated erosion is generally short lived, typically less than a decade, resulting in significant, but unquantified, volumes of sediment remaining in the orogen after sediment discharges have returned to previous levels. As many coseismic landslides occur in bedrock much of the sediment within their deposits is too coarse to be transported by suspension resulting in aggradation of channels for decades after an earthquake (Pearce and Watson 1986; Koi et al. 2008; Vanmaercke et al. 2017). This coarse sediment must be transported by bedload processes and is likely to remain in the landscape for hundreds of years. Empirical estimates of bedload transport estimate that the sediment from the 1999 Chi Chi earthquake in Taiwan could take 250-600 years to be fully evacuated from the landscape (Yanites et al. 2010). Detailed dating and mapping of the Pokhara region in Nepal also suggests river system can rework sediment from large earthquakes for several hundred years (Schwanghart et al. 2016; Stolle et al. 2017; Stolle et al. 2019).

Alongside the residence time of sediment in the fluvial system, we must also consider possible storage of sediment on the hillslope. Small landslide deposits can be deposited on the hillslope far from the river or deposited in channels which lack the discharge to consistently erode them (Pearce and Watson 1986; Li et al. 2016; Roback et al. 2018). Landslides disconnected from the channel network cannot be actively reworked by undercutting and therefore must be eroded into the channel network by diffusive processes or stochastically by debris flows, which could significantly increase their residence times (Vanmaercke et al. 2014; Zhang and Zhang 2017; Fan et al. 2019b). Attempting to include connectivity in dynamic models of sediment transport is difficult due to the rates and initiation mechanisms of these processes being unknown in many locations. However, simple statistical numerical modelling suggests that unconnected landslide deposits could extend the period of time impacted by the earthquake by hundreds or thousands of years (Croissant et al. 2019; Francis et al. 2020).

Satellite imagery with high spatial and temporal resolution allows for the monitoring of large areas of mountain ranges. These can be used to generate multi-temporal landslide inventories after major earthquakes to understand the spatio-temporal evolution of post seismic mass wasting processes (Marc et al. 2015; Tang et al. 2016; Zhang and Zhang 2017; Kincey et al. 2021). Multi-temporal inventories can provide a link between long term sedimentary (Stolle et al. 2019) and short term suspended sediment discharge records (Lin et al. 2008) by helping to identify the key sediment transport processes. Here we use a multitemporal landslide inventory of the 2008 Mw 7.9 Wenchuan earthquake to generate the first sediment budget of a large earthquake. We use this sediment budget to determine the key sediment transport processes in the post seismic landscape and to pose questions about the long-term evolution of the epicentral area.

1.2 The Longmen Shan and the 2008 M_w7.9 Wenchuan earthquake

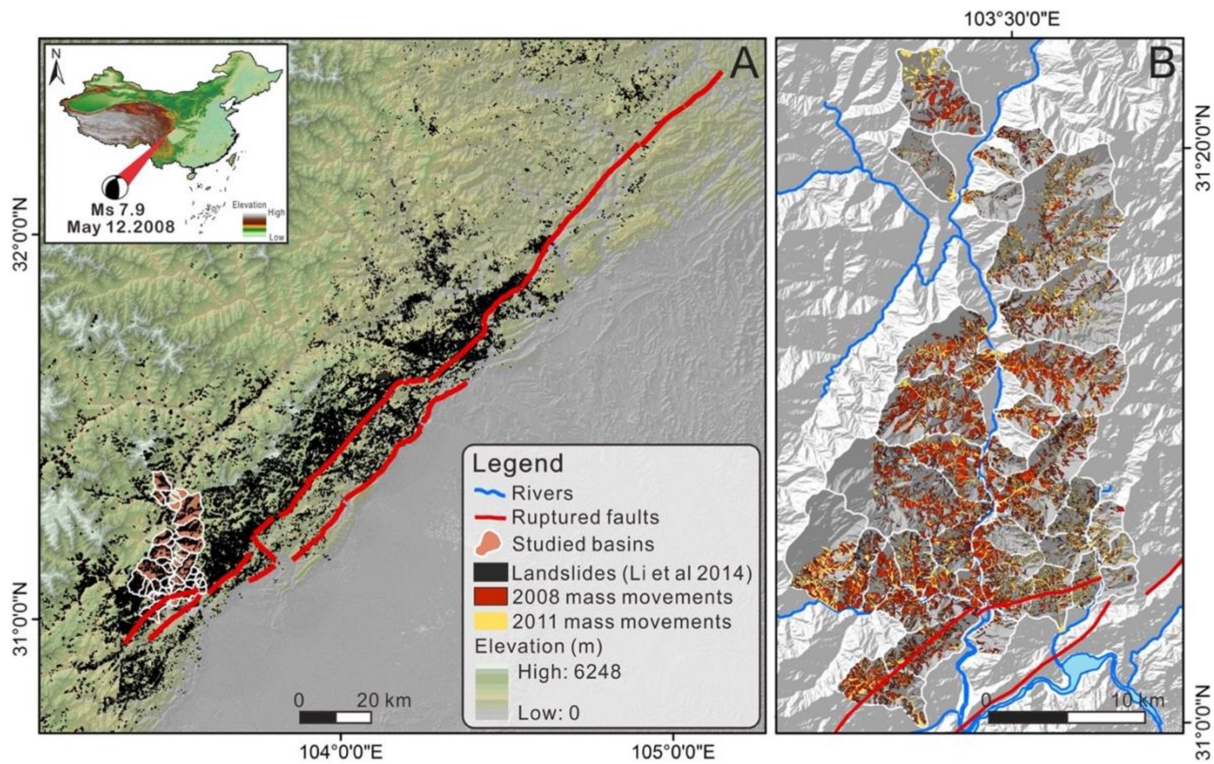

Figure 1. A) The surface rupture of the earthquake in red with the landslides in black. Note the highest densities of landslides area found close to the ruptures. The inset shows the location of the earthquake on the eastern margin of the Tibetan Plateau and the edge of the Sichuan Basin. The catchments highlighted in white are the catchments studied in this paper. B) The studied catchments with the Min Jiang running north to south through the middle of the image. The coseismic mass movements are mapped in red while the post seismic (between 2008 and 2011) movements are in yellow.

On the 12th May 2008 the country of Wenchuan in the Chinese province of Sichuan was shaken by a magnitude M_w7.9 earthquake. The earthquake occurred along the Longmen Shan thrust zone, which separates the Longmen Shan mountain range from the Sichuan Basin, and ruptured 2 major faults for over a hundred kilometres (Figure 1) (Liu-Zeng et al. 2009; Densmore et al. 2010). The earthquake triggered more than 60,000 landslides across an area of 35,000 km^2 (Huang and Fan 2013; Li et al. 2014) making it one of the most erosive earthquakes on record (Marc et al. 2016a). Coseismic landsliding is found in the greatest densities close to the traces of the ruptured faults with areal densities of up to 9.6% (Dai et al. 2011). Areas around the fault zone have weaker rock strength than expected of fresh bedrock (Gallen et al. 2015) and higher denudation rates than the rest of the landscape, suggesting frequent earthquakes have conditioned the area resulting in rapid erosion rates (Li et al. 2017).

The Longmen Shan is one of the steepest mountain ranges in the world, the frontal range rapidly increases in elevation from 500 – 4000m over distances of just 50km (Kirby and Ouimet 2011). The mountain range is the eastern margin of the Tibetan Plateau and as a result is an area of complex tectonic and geodynamic activity (Burchfiel et al. 2008; Royden et al. 2008; Hubbard and Shaw 2009). The high mountain peaks are dissected by deeply incised valleys and gorges of the rivers draining the mountain range (Densmore et al. 2007; Kirby and Ouimet 2011). The Min Jiang, the major river draining the epicentral area, is bordered with several layers of terraces which record the long term uplift and incision of the area (Godard et al. 2010). The main trunk of the river has a characteristic width of 100m while many of the tributary catchments which drain into the river in the epicentral region of the earthquake are significantly smaller (Figure 2A). Rainfall is highly variable across the mountain range with the highest annual precipitation (800 – 1200mm) found right on the mountain front (Guo et al. 2016). Rainfall and river discharge also vary temporally, the monsoon season between May and October is responsible for the majority of the rainfall and discharge (Wang et al. 2015). Mass movements are common in the Longmen Shan due to the steep hillslopes and high frequency of intense rain storms in the mountain range (Ouimet et al. 2007; Ouimet et al. 2009).

Following the earthquake coseismic landslide sediment immediately began to be remobilised and reworked by the fluvial system. Suspended sediment discharges in the Min Jiang, and other rivers, increased by an order of magnitude (Wang et al. 2015), while the concentrations of cosmogenic ^{10}Be in detrital sediment dramatically declined (West et al. 2014; Wang et al. 2017). On average these records show that sediment transport has or is returning rapidly to pre-earthquake levels in the years since. However, there is significant variation in this pattern which is primarily linked to the landslide density in individual catchments. Catchments with higher landslide densities and more frequent large rainstorms tend to produce larger and longer lasting increases in sediment discharge (Wang et al. 2015; Wang et al. 2017). These increases seem to be unaffected by the volume of sediment connected to channel network. Around 40% of the total coseismic landslide sediment volume is connected to the channel network but suspended sediment discharge remains high even in locations with low connectivity (Li et al. 2016). The lack of a correlation between suspended sediment discharge and connectivity could be an indicator of the high mobility of fine sediment immediately after the earthquake.

The most striking indicator of the earthquake significantly impacting the sediment transport rates of the area is the occurrence of huge (mobilising >10^6 m^3 of sediment) debris flows (Tang et al. 2012). These are some of the largest debris flows ever observed and have occurred with frequencies rarely seen elsewhere (Korup 2012). The debris flows occurred in the smaller tributary catchments of the Min Jiang where high landslide densities are common and significant aggradation of the channel bed is observed (Zhang and Zhang 2017) (Figure 2b). These large debris flows are the single largest part of the stochastic sediment cascades (Bennett et al. 2014; Zhang and Zhang 2017). Understanding these events in the context of other smaller processes in a sediment budget is important to determine the likely future of the area.

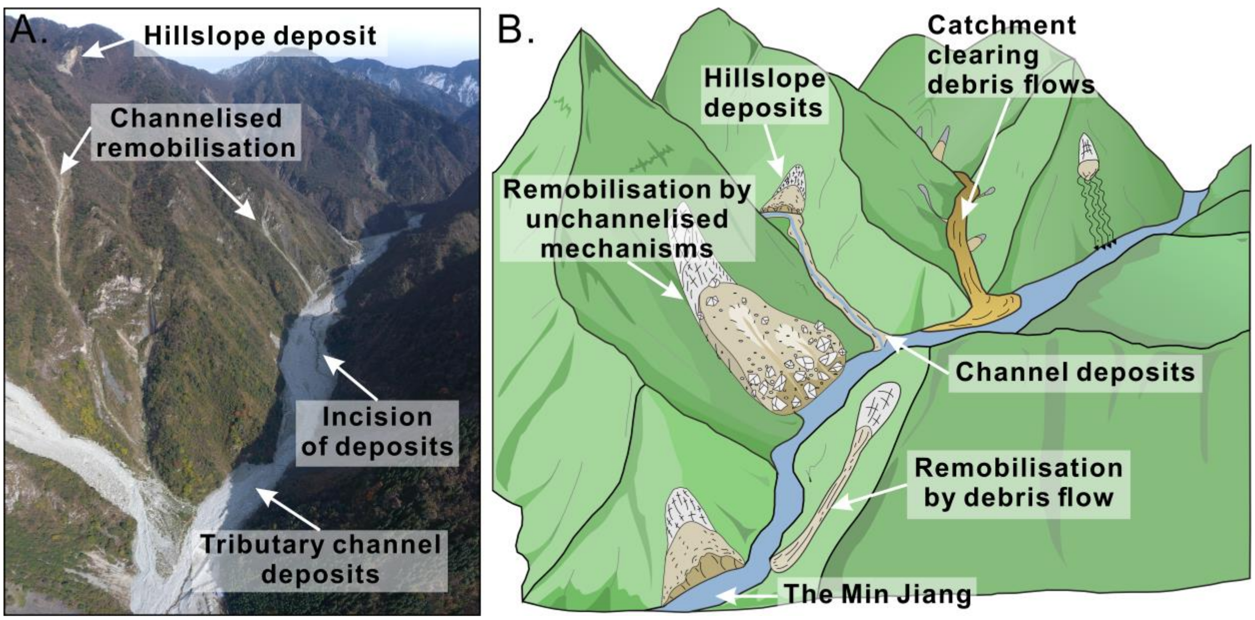

Figure 2. A) Drone image of a subcatchment of the Min Jiang, taken in October 2019. The main sediment storage types are highlighted as well as the visible signs of sediment transport. B) A conceptual cartoon of the Min Jiang following the earthquake. The main sediment transport processes are represented along with their sources and sinks.

2 Materials and Methods

2.1 Study area and structure of the sediment budget

Our sediment budget covers the reach of the Min Jiang between the towns of Yingxu, close to the epicentre of the earthquake, and Wenchuan town (Figure 1). The study focused on the 28 catchments which discharge directly into the main trunk of the Min Jiang (Figure 1B). We mapped the coseismic and postseismic landslides between 2008 and 2018 to estimate the volume of sediment that moved from the hillslope into the Min Jiang during this period. Using the multitemporal inventories we identified the key sediment transfers and stores within our study area.

2.2 Multitemporal landslide inventory

The multitemporal landslide inventory is the basis of our sediment budget as it constrains the volume of sediment generated during our study period and the transfer of sediment from the hillslope to the channel network. This inventory is an adapted version of the inventory described in Fan et al. (2019b), here we will briefly describe the methodology used to generate this inventory and the key alterations we made.

The inventory is derived from orthorectified satellite (and some aerial) imagery of 6 different years after the earthquake (Table S1). The 2011 image provided coverage of the entire area in high resolution and hence was chosen as the geo-referencing base for the study. Each image was orthorectified using the Pix4D software before detailed checks were employed to ensure there were no major rectifying errors between the inventories (Williams et al. 2018). In each image we visually mapped any new mass movements along with any remobilisation within the mass movements mapped in a previous image. Mass movements were mapped as polygons which covered the entire area of the mass movement, no effort was made to separate the source and deposition areas. New mass movements were identified by the stripping of vegetation from the hillslope which do not intersect with any previous mass movements. Remobilisation was mapped by identifying changes within previously mapped mass movements (Figure S1). These changes could be the formation of rill networks, debris flows or landslide scars, or the clear movement of boulders. Any mass movement which intersected with a previously mapped mass movement was classified as a remobilisation due its final volume likely including entrained previously deposited sediment. This classification system differs from the ‘activity level’ used in original inventory where landslides are classified by the area of the polygon not covered by vegetation (Tang et al. 2016; Fan et al. 2019c). Our mapping scheme allowed us to directly map the area of the remobilisation which we then used as the base of our sediment budget.

Within this mapping scheme we classified two processes in each epoch; landslides and debris flows using the definitions of Fan et al. (2018) (Figure S1). This classification was determined visually based upon the shape of the mapped polygons. Debris flows polygons are long and thin possibly with visible leeves while landslides are wide with no channelisation visible. We also classified remobilisation using a similar scheme, however as less data exists for these processes, we used more generalised terms. Remobilisation polygons which are long and thin were classified as channelised remobilisation (debris flows). Remobilisation polygons without any clear channelisation were defined as unchannelised, these can be formed by shallow landsliding within a previous deposit or may be produced by a dense, impossible to resolve from the imagery, rill network (Figure 1).

2.3 Literature review derived processes and volumes

Alongside the processes identified in the multitemporal landslide inventory we conducted a review of the post Wenchuan earthquake literature to identify other processes which are taking place in the area. These are described below:

Catchment clearing debris flows are large debris flows which evacuate volumes of sediment from the hillslope and tributary channels directly into the Min Jiang. The volumes of these processes were quantified from the database of debris flow events collated by Fan et al. (2019b). This database consists of any large debris flow event recorded in technical reports or papers, most of which had reported volumes of the deposition fan of the event. As uncertainty data was unavailable for most of the events, we assumed ± 50% of the reported volume. The volume of the debris flow was assumed include an even mixture of hillslope and tributary channel deposit material.

Overland flow erosion of mass movements is an estimate of the volume of sediment removed from bare sediment by runoff. We estimated the volume removed by this process using the field measurements performed by Fusun et al (2013). They deployed sediment traps to record the volume of sediment leaving landslides over a monsoon period and reported their results in the form g/m^2. We used these results and extrapolated them, assuming a constant erosion rate, across the active bare area of the mass movements for each time step. Uncertainty was calculated using a range of bulk densities for the coseismically generated sediment as well as the range of field recorded erosion rates.

Suspended sediment is also included in our budget as a separate process as it is one of the only records of sediment transport and erosion in the channel network. The suspended sediment discharge is calculated from the measurements reported by Wang et al. (2015). Using daily records of suspended sediment concentration and water discharge Wang et al. (2015) calculated the increase in sediment transported by the rivers draining the orogen after the earthquake. We assumed the increase in sediment discharge was related to the volume of sediment upstream of the recording station and thus scaled the increase by the volume of sediment in our study area. We kept the discharge constant throughout time as the processes behind the timescale of the enhancement are unknown. Uncertainty in our values is as reported in Wang et al. (2015).

3 Constructing the sediment budget

3.1 Volume estimates of coseismic and post seismic landslides

The mapped area of coseismic landslides is commonly converted into an estimated volume using the empirical area-volume scaling relationship ($V = \alpha A^{Y}$ where V is the volume of the landslide, A is its mapped area and α and Y are empirical parameters). As the volume of only a small number of landslides has ever been measured these scaling parameters have significant uncertainty (Larsen et al. 2010; Li et al. 2014). Due to this uncertainty, and the small number of landslide volume measurements in the Wenchuan epicentral area, we use the methodology proposed by Li et al. (2014) to calculate the volume of our mapped co- and post-seismic landslides. This method uses a Monte Carlo simulation of six sets of scaling parameters to estimate the total landsliding volume of an epoch and its uncertainty. Each simulation uses a randomly chosen α and Y values for each polygon from a normal distribution limited by the uncertainty stated in table 1. We ran 50,000 Monte Carlo simulations for each of the scaling relationships and calculated the total landsliding volume for each simulation. We then calculated the median, 16^{th} and 84^{th} quartiles of the simulations to determine the total landsliding volume and its uncertainty. The combined volume estimate is derived from a dataset of all the results of the simulations of the scaling relationships.

Reference	$Log_{10}\alpha$	*Y*	Total Coseismic Volume (km^3)	Total Post Seismic Volume (km^3)
(Larsen et al. 2010)	-0.836 ±0.015	1.332 ±0.005	6 ×10-1 ($\pm1\times10^{-3}$)	3×10^{-3} ($\pm 3\times10^{-5}$)
(Larsen et al. 2010)	-0.73 ±0.06	1.35 ±0.01	1 ($\pm1\times10^{-3}$)	4×10^{-3} ($\pm1\times10^{-4}$)
(Larsen et al. 2010)	-0.59 ±0.03	1.36 ±0.01	1 ($\pm7\times10^{-3}$)	7×10^{-3} ($\pm1\times10^{-4}$)
(Guzzetti et al. 2009)	-1.131	1.45 ±0.009	1 ($\pm4\times10^{-3}$)	4×10^{-3} ($\pm7\times10^{-5}$)
(Parker et al. 2011)	-0.974 ±0.366	1.388 ±0.087	2 ($\pm1\times10^{-1}$)	6×10^{-3} ($-1/+2\times10^{-3}$)
(Li et al. 2014)	-0.995 ±0.366	1.392 ±0.087	2 ($\pm1\times10^{-1}$)	6×10^{-3} ($-1/+2\times10^{-3}$)
Combined			1 ($-6/+5\times10^{-1}$)	5×10^{-3} ($\pm2\times10^{-3}$)

Table 1. The results of the Monte Carlo Simulations. Each set of parameters is run 50,000 times and combined to produce an overall estimate of total volume and uncertainty. Coseismic volume includes all landslides that are mapped in the 2008 image while the post-seismic volume includes all new landslides mapped after this year.

3.2 Estimating the volume of tributary channel deposits

In order to constrain the volume of sediment entering the channel between each image we first produced an independent estimate of the sediment stored. This estimate is then compared to the estimates of sediment transfer produced by the sediment budget in order to identify and dismiss inappropriate area – volume scaling parameters. If a set of parameters produces an estimate of sediment transfer from the hillslope to the channel network significantly outside of the range produced by the independent estimate it is removed from consideration (Table S2).

This independent budget of the tributary channel deposits was constructed by mapping the cross-sectional width of the active channel deposits in the tributary catchments. The cross-sectional width was defined as the border of sediment from one side of the channel to the other (Figure S2). This width was then mapped at regular intervals for each catchment in each epoch. During times of deposition these widths would increase while during times of low sediment input, they would remain relatively stable.

To estimate the volume of the channel deposits we simply assumed a triangular cross-sectional area and interpolated across the distance between the cross-section locations. Each time an increase in width was recorded we assumed a corresponding increase in the depth of the deposit and subtracted the previous volume to estimate the change in stored volume over the epoch (Figure S3). As we were unable to map the angle of the base of catchment hillslopes, we used slope angles of 20 and 40 to determine the cross-sectional area. Therefore, the minimum estimate assumes a deposit side angle of 20 degrees while the maximum assumes an angle of 40 for each cross section.

During times of minimal deposition, we estimated the volume of sediment that is removed from the channel deposits by reworking by the channel. For this we simply measured the width of the actively incising channel and again assumed a triangular cross section. For the bank angles of the channel we used the angle of repose of landslide deposits estimated by Wang et al. (2013). As debris flows are also active in the tributary channel deposits and we could not separate the effects of these and fluvial erosion we term this erosion incision.

3.3 Transfer of sediment between hillslope and channels

While there are several empirical area – volume scaling relationships for landslides it is unclear whether they are suitable for use with debris flows and remobilisations (Marc and Hovius 2015). To determine the volume of sediment entering the channel deposits we tested a variety of scaling equations using the Monte Carlo method described earlier and compared them to our independent estimate of channel deposit volume (Table S2). Any scaling relationships which produce total volume estimates outside of the independent range are removed from the Monte Carlo simulations.

To determine whether a mass movement transfers sediment into the tributary channel deposits we compared the maximum drainage area of the mapped polygon with a hillslope/channel threshold. This threshold was derived from a threshold based channel extraction algorithm in the software LSDTopoTools (Mudd et al. 2020). An initial estimate of a threshold was derived from mapping likely channel head locations in satellite imagery. However due to the uncertainty in this approach we created a new threshold from the extracted channel network by determining the median drainage area of a first order channel. If a remobilisation shapefile had a drainage area greater than this threshold it is assigned to the tributary channel deposits. We also calculated the median drainage area of larger order streams in order to determine whether sediment was deposited directly into the Min Jiang.

Using this methodology, we concluded that remobilisation shapefiles and new mass movement shapefiles need separate area – volume scalings. The landslide area-volume scaling relationships used previously (Table 1) considerably overestimate the volume of sediment mobilised and were therefore excluded from consideration (Table S2). Instead we used a combination of the shallow soil landslide scaling derived by Larsen et al. (2010) ($\mathrm{Log}_{10}\alpha = -0.836 \pm 0.015$, $Y = 1.145 \pm 0.008$) and average depths between 0.05 and 0.95m.

3.4 Sources and stores

To finalise our budget we must identify the sources and stores of each identified process. A key observation of our multitemporal landslide inventory is that the channel network does minimal erosion to landslide deposits which were not directly deposited into the Min Jiang. Minimal undercutting of landslide deposits was observed in the field and satellite imagery suggesting that hillslope processes are the main way by which landslides are eroded. The tributary channels are small and do not have the transport capacity to mobilise the coarse sediment of the deposits. Therefore in our sediment budget all landslides are initially added to the hillslope deposit store unless they are deposited directly into the Min Jiang. Debris flows by contrast can deposit directly into the tributary channel deposits (or the Min Jiang) as their mobility is great enough allows them to travel along the channel before depositing.

All remobilisation processes from the hillslope can deposit in any store depending on the mobility of the mass movement and the original location of the source sediment. Catchment clearing debris flows can be triggered by remobilisation from the hillslope, run off with in the channel, or the merging of multiple debris flows (Tang et al. 2012; Cui et al. 2013). Due to the complexity in triggering we simply assume the final volume of the deposit comes equally from the hillslope and the tributary channels.

4 Results

4.1 Full post-earthquake sediment budget

In the study area, we mapped a total of 15,130 mass movements (8,830 coseismic and 6,300 post seismic) across the study period (Fig 1B). These mass movements generated a total volume of 1.1 (±0.5) km^3 of sediment. 96% of the sediment was generated coseismically, indicating any post seismic enhancement of landsliding is not a significant contributor to post seismic sediment discharges. Of the sediment that was mobilised from the hillslope after the earthquake, less than 1% was from new post seismic mass movements suggesting the increase in sediment discharge records is almost exclusively driven by remobilisation of coseismic sediment. Nearly half of the sediment deposited into the Min Jiang, 48.1% (1.9×10^{-2} -8.5/+7.6×10^{-3} km^3), was from coseismic landslide material deposited directly into the river (Table 2). The majority of sediment deposited into the Min Jiang after the earthquake came from the tributary channel deposits. Just 8.1% (1.6×10^{-3} -3×10^{-4}/+6.9×10^{-3} km^3) of the sediment postseismically deposited into the Min Jiang was done so directly from hillslope deposits. Therefore the sediment cascade is the primary way by which sediment is evacuated from the orogen.

At the end of the decade long study, we found that 93.8% (-6.2+0.3%) of the sediment generated during and after the earthquake remains on the hillslope. 2.8% (-0.8/+6%) is found in the tributary channel deposits and the final 3.4% (+0.5%) has been deposited into the Min Jiang (Figure 3). Of the sediment that was deposited on the hillslope during the earthquake 95.7% remains. 85.4% (4×10^{-2} -2.2×10^{-2}/+1.1×10^{-1} km^3) of the sediment is remobilised from the hillslope is deposited into the tributary channel deposits where it requires further remobilisation before it is evacuated from the orogen.

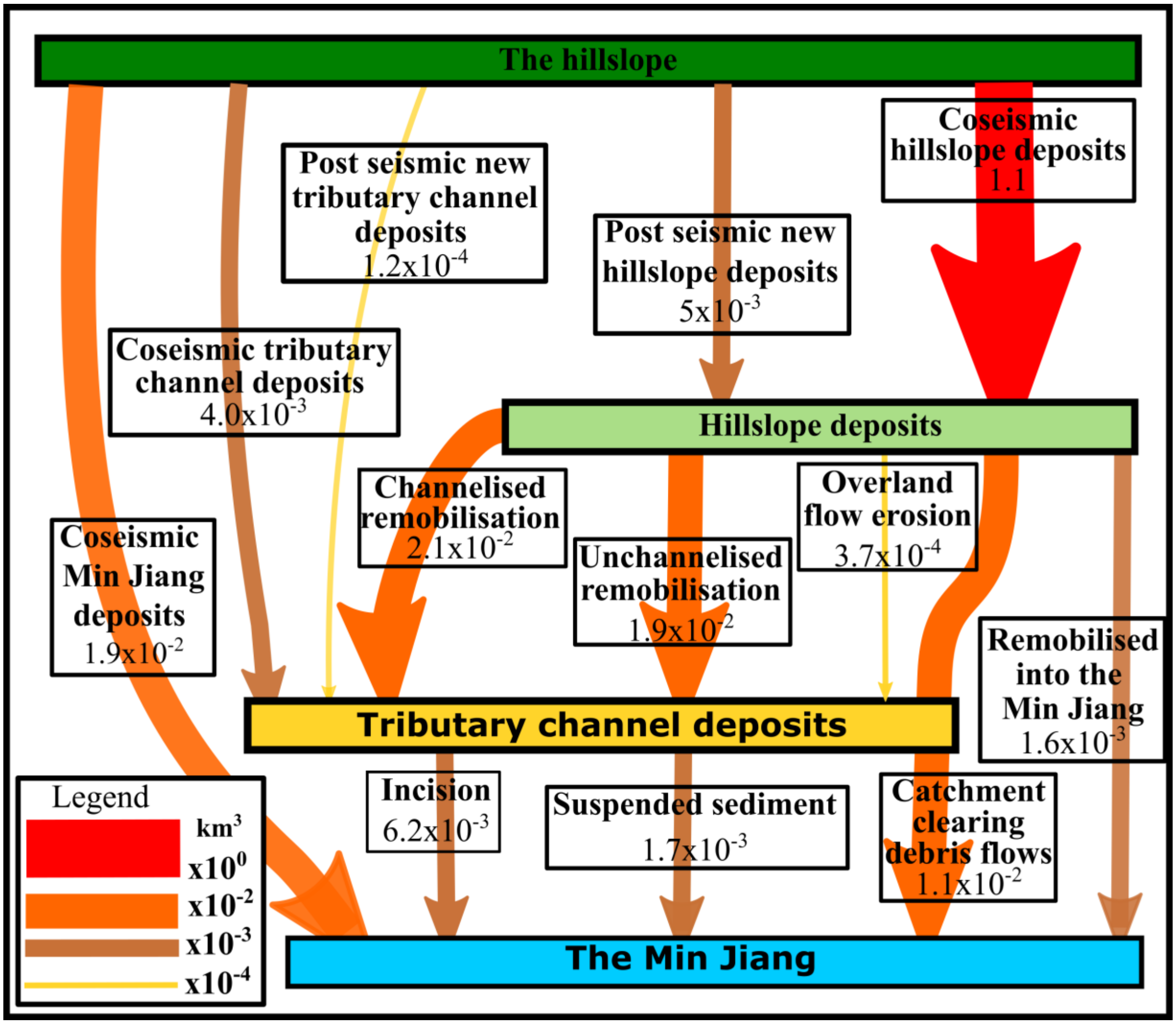

Figure 3. The sediment budget of the Wenchuan Earthquake. The width and colour of each arrow indicates the magnitude of the sediment moved by the process between the stores. Catchment clearing debris flows erode sediment from both hillslope and tributary channel deposits and is represented by an arrow passing through the tributary channel deposits in a single motion. The budget is also shown in table form in Table 2.

Large catchment clearing debris flows are the major process depositing sediment into the Min Jiang accounting for 52.4% ($1.1\times10^{-2} \pm 5.2\times10^{-3}$ km^3) of the sediment deposited into the river after the earthquake. Debris flows (both small channelised remobilisations and large catchment clearing flows) dominate the sediment budget accounting for 50% (3.3×10^{-2} $-1.6/+7.5\times10^{-2}$ km^3) of all sediment mobilised. Fluvial processes (here represented by incision and suspended sediment), on the other hand, are only minor contributors to sediment transport over our study period.

Coseismic sediment budget	**Volume (km^3)**	**Uncertainty (km^3)**	**%**
Coseismic hillslope deposits	1.1	± 0.53	97.5
Coseismic tributary channel deposits	4.0×10^{-3}	$-1.8\times10^{-3}/+1.4\times10^{-2}$	0.4
Coseismic Min Jiang deposits	1.9×10^{-2}	$-8.5/+7.6\times10^{-3}$	1.6
Post-seismic new landslides and debris flows			
Post seismic new hillslope deposits	5.0×10^{-3}	$-1.8/+4.2\times10^{-3}$	0.4
Post seismic new tributary channel deposits	1.2×10^{-4}	$-2.2\times10^{-5}/+7.8\times10^{-4}$	0.0
Total sediment generated	**1.13**	± 0.55	
Remobilisation of hillslope deposits			
Channelised remobilisation	2.1×10^{-2}	$-1/+6.3\times10^{-2}$	1.8
Unchannelised remobilisation	1.9×10^{-2}	$-1.2/+4.4\times10^{-2}$	1.7
Into the Min Jiang	1.6×10^{-3}	$-3\times10^{-4}/+6.9\times10^{-3}$	0.1
Overland flow erosion	3.7×10^{-4}	$\pm7.3\times10^{5}$	0.0
Remobilisation of channel deposits			
Catchment clearing debris flows	1.1×10^{-2}	$\pm5.23\times10^{-3}$	0.9
Suspended sediment	1.7×10^{-3}	$-7\times10^{-4}/+1.2\times10^{-3}$	0.2
Incision	6.2×10^{-3}	$\pm1.01\times10^{-3}$	0.6
Stores			
Hillslope deposits	1.06	-0.5/+0.4	93.8
Tributary channel deposits	3.1×10^{-2}	$-2\times10^{-2}/+1.2\times10^{-1}$	2.8
Min Jiang	3.9×10^{-2}	$-1.6/+2.2\times10^{-2}$	3.4

Table 2. The full sediment budget from figure 3 in table form. All values are rounded to 1 significant figure. The percentage values are derived from the median value of each process and the total sediment generated.

4.2 The sediment budget through time

Using the satellite images we can separate the budget into 4 epochs (2008 – 2011, 2011 – 2013, 2013 – 2015, and 2015 – 2018) to analyse how the processes and overall discharge changes through time. We find that the average total discharge (the sum of all processes) decreases by an order of magnitude from 1.4×10^{-2} (-7.8×10^{-3}/$+2.7\times10^{-2}$) – 1×10^{-3} (-2.7×10^{-4}/$+7.5\times10^{-4}$) km^3/year (Table 3). A total of 6.4×10^{-2} (-3.1×10^{-2}/$+1.3\times10^{-1}$) km^3 of sediment (both new and remobilised coseismically generated) is mobilised after the earthquake, 90.8% of which was mobilised during the first 5 years after the earthquake. The total sediment discharge decreases rapidly until 2015 after which it begins to level off suggesting it had begun to stabilise by the end of the study period.

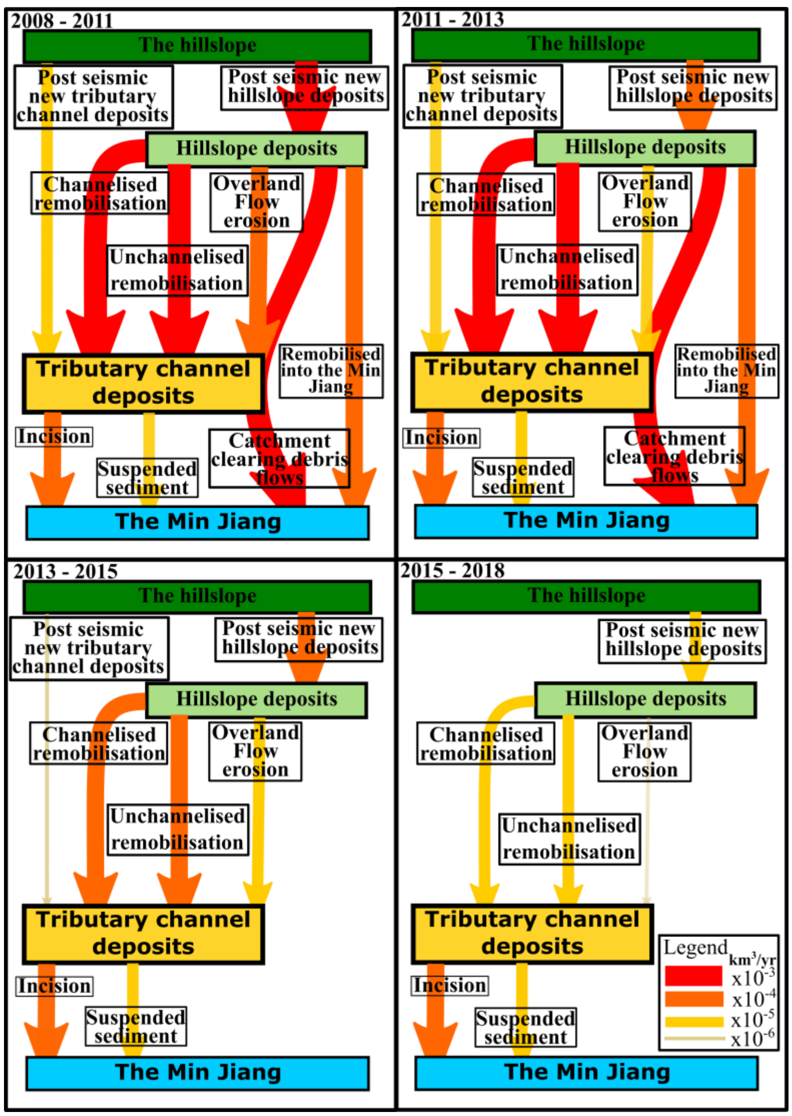

Figure 4. The sediment budget separated into the 4 postseismic epochs. Numbers in the store labels describe the average yearly sediment budget for that store (km^3/yr). The thickness of the arow reflects the magnitude of the sediment transfer while the colour represents the source of the sediment. If a transfer path becomes inactive during a particular epoch the arrow is removed from the diagram.

The rate at which the hillslope deposits are depleted decreases by 3 orders of magnitude from 1.1×10^{-2} (-6.4×10^{-3}/$+2.54\times10^{-2}$) – 4.7×10^{-5} (-2.9×10^{-5}/$+5\times10^{-4}$) km^3/year over our study period. For each epoch the volume of sediment produced by postseismic mass movements (new landsliding and debris flows) is less than the volume remobilised from the hillslope deposits. This decrease in remobilisation rates coincides with the overall decrease in sediment discharge. As remobilisation of coseismic deposits continues to dominate the hillslope sediment discharge at the end of our study period, it is likely the overall discharge remains elevated above pre-earthquake levels.

Tributary channels have aggraded due to the high volumes of sediment deposited into them. Only after 2013 do the tributary channel deposits erode rather than aggrade. This is despite the major eroding process of the tributary channel deposits, the catchment clearing debris flows, ceasing to occur within our study area. The major cause of the negative tributary channel deposit budget seems to be due to a decrease in the volume of sediment being deposited within the channels. A slight increase in the volume of sediment leaving the deposits via incision is seen, however due to a lack of constraints we are not able to verify this pattern. If the deposition of sediment into the tributary channel deposits remains low it is likely the total volume of sediment stored will continue to decrease.

Finally, we see an overall decrease in the volume of sediment entering the Min Jiang due to the ceasing of large catchment clearing debris flows. Without these large flows the volume of sediment entering the Min Jiang decreases by an order of magnitude, highlighting the importance of the largest events to evacuating the coseismic sediment from the Longmen Shan.

All units km^3/yr	2008 -2011	2011-2013	2013-2015	2015 - 2018
Post-seismic new landslides and debris flows				
Post seismic new hillslope deposits	1.1×10^{-3} ($-4/9\times10^{-4}$)	6.4×10^{-4} ($-2.3/+5.7\times10^{-4}$)	1.4×10^{-4} ($-4.8\times10^{5}/+1.4\times10^{4}$)	4×10^{-5} ($-1.3/+2.4\times10^{-5}$)
Post seismic new tributary channel deposits	2.6×10^{-5} ($-4.8\times10^{-6}/+1.5\times10^{-4}$)	2.1×10^{-5} ($-3.5\times10^{-6}/+1.7\times10^{-4}$)	3.6×10^{-6} ($-5.7\times10^{-7}/+2.8\times10^{-5}$)	0
Remobilisation of hillslope deposits				
Channelised remobilisation	4.9×10^{-3} ($-2.6\times10^{-3}/+1.3\times10^{-2}$)	2.5×10^{-3} ($-1/+9\times10^{-3}$)	4.0×10^{-4} ($-8\times10^{-5}/+2.2\times10^{-3}$)	2.2×10^{-5} ($-4\times10^{-6}/+1.24\times10^{-4}$)
Unchannelised remobilisation	5×10^{-3} ($-3.3\times10^{-3}/+1\times10^{-2}$)	1.9×10^{-3} ($-1.1/+5.6\times10^{-3}$)	1.3×10^{-4} ($-4.1/6.7\times10^{-4}$)	6.2×10^{-5} ($-1.1\times10^{-5}/+3.6\times10^{-4}$)
Into the Min Jiang	2.7×10^{-4} ($-5\times10^{-5}/+1.1\times10^{-3}$)	4.1×10^{-4} ($-7.5\times10^{-5}/+1.7\times10^{-3}$)	0	0
Overland Flow erosion	2.9×10^{-4} ($\pm5.6\times10^{-5}$)	5.8×10^{-5} ($\pm1.13\times10^{-5}$)	2.2×10^{-5} ($\pm4.3\times10^{-6}$)	3.1×10^{-6} ($\pm6\times10^{-7}$)
Remobilisation of Channel deposits				
Catchment clearing debris flows	2.5×10^{-3} ($\pm1.3\times10^{-3}$)	1.4×10^{-3} ($\pm7.1\times10^{-4}$)	0	0
Suspended sediment	5.3×10^{-5} ($\pm2.3\times10^{-5}$)	5.3×10^{-5} ($\pm2.3\times10^{-5}$)	5.3×10^{-5} ($\pm2.3\times10^{-5}$)	5.3×10^{-5} ($\pm2.3\times10^{-5}$)
Incision	1.9×10^{-4} ($\pm5\times10^{-5}$)	4.9×10^{-4} ($\pm1.3\times10^{-4}$)	6.8×10^{-4} ($\pm1.8\times10^{-4}$)	8.3×10^{-4} ($\pm2.2\times10^{-4}$)

Table 3. The sediment budget separated into 4 epochs with each process quantified and averaged across the epoch. All units are in km^3/yr

5 Discussion

Our full sediment budget of the Wenchuan earthquake reveals that over 90% of the sediment produced by the earthquake remains on the hillslope 10 years after the earthquake. The majority of the coseismically generated sediment is mobilized by debris flows, either small flows which deposit sediment to the base of the hillslope or rare large flows which can bypass the tributary channel deposits and mobilise sediment directly into the Min Jiang. While the largest catchment clearing debris flows are relatively frequent during the first few years after the earthquake it is unlikely they will continue occur as often as this in the future. This suggests that most sediment will have to pass through the tributary channel deposit store before it is mobilised out of the system. This pattern of remobilisation and deposition could be repeated multiple times likely extending the residence time of some sediment up to 100s if not 1000s of years.

Our sediment budget also demonstrates that the rate at which sediment is remobilised from the hillslope has decreased since the earthquake. In the first epoch (2008-2011) of our budget we recorded 4296 remobilisation events, 1193 of which were channelised. However, in the final epoch (2015-2018) just 54 remobilisations were recorded (11 channelised). Despite there being more unchannelised remobilisations than channelised, channelised remobilisations more frequently deposited sediment into the channel network due to their longer runouts making them near equal contributors. This rapid reduction in remobilisation frequency is most likely due to a stabilisation of the hillslope deposits rather than exhaustion due to the large volume of sediment remaining on the hillslope. This apparent stabilisation of the hillslope deposits will also extend the residence time of coseismically generated sediment beyond that of what can be expected from rates recorded here. The reduction in debris flow frequency we observe is also reported in other studies; rainfall intensity duration thresholds in the epicentral area have increased since the earthquake leading to indications of a stabilisation of the coseismically generated sediment taking place (Zhang and Zhang 2017; Fan et al. 2020).

The mechanisms behind this apparent stabilisation are still unknown, however there are several theories which we will discuss here. The first is that colonisation of the landslide area by vegetation has increased the resistive strength of the landslide deposit. Depending on the triggering mechanism of the failure vegetation can stabilise the deposit in several ways. The canopy of vegetation can intercept the rainfall before it strikes the sediment reducing the local intensity and saturation state (Wilkinson et al. 2002; McGuire et al. 2016). While the trunks and stems of vegetation increase the roughness of the slope reducing the speed of any potential surface runoff reducing the stress applied to the sediment. Vegetation can suck water out and increase the shear strength of the soil increasing the intensity required to produce failure through saturation (Hales et al. 2009; Hales 2018). Vegetation is seem as a contender to stabilising the coseismically generated sediment due to satellite observations which show that NDVI (Normalised Difference Vegetation Index) values are returning rapidly to pre-earthquake levels (Shen et al. 2020; Yunus et al. 2020). This rebound in vegetated area appears to be well correlated with a reduction in remobilisation of sediment (Fan et al. 2018; Yunus et al. 2020). However the first vegetation to colonise the landslide areas tend to be grasses and shrubs (Shen et al. 2020), most of which only have shallow and weak root structures which do not add significant strength to the sediment (Hales 2018). Therefore if saturation is the main way by which debris flows and landslides occur within the coseismically generated sediment it is unlikely vegetation is the main mechanism by which the sediment is stabilised. If instead surface runoff is the main way by which sediment is remobilised it is possible grasses and shrubs may slow runoff enough to prevent debris flows from occurring. However it is currently unclear how remobilisation is triggered in hillslope deposits but it is unlikely vegetation is the only mechanism by which sediment is stabilised.

The other mechanism which has been proposed to explain the stabilisation of the hillslope deposits is internal erosion which preferentially removes fine sediment from the deposits (Cui et al. 2014; Hu et al. 2016; Hu et al. 2017; Zhang and Zhang 2017). It is hypothesised that fresh landslide deposits are highly permeable which allows water to pass through easily. As the water passes through the deposit it can entrain the fine sediment and transport it out of the deposit. This muddy mixture can then induce localised failures within the deposit in less permeable parts of the deposit (Cui et al. 2014). If enough of these small failures occur it is possible a debris flow can be formed. However if no large scale failure occurs the deposit will be left in a fines depleted state which is more porous and permeable and as a result less favourable for failure in the future (Hu et al. 2016; Hu et al. 2017). The smaller failures may also compact the deposits which has also been shown to reduce the likelihood of failure in loose sediment (Iverson et al. 2000; Gabet and Mudd 2006; Chang et al. 2011). However, there is minimal in situ evidence for this theory of preferential erosion of fine sediment. The primary source of field evidence for this coarsening is from debris flow deposit sequences (Chen et al. 2014; Zhang et al. 2014; Yang et al. 2021). The newer debris flow deposits are significantly coarser than the older deposits, however it is not clear whether the patterns in the deposit reflect the processes occurring in the source. Finally, for this coarsening process to be a significant factor in the stabilisation of hillslope deposits across the area it is likely vast volumes of fine sediment would have to be mobilized and deposited into the Min Jiang. However, the suspended sediment discharge of the river returned to pre-earthquake levels before significant volumes of sediment could be mobilised (Wang et al. 2015).

Small debris flows are the major process in remobilising sediment from the hillslope into the tributary channel deposits while large catchment clearing debris flows are the main process by which sediment is deposited into the Min Jiang. After 2013 there are no large catchment clearing debris flows and as a result the volume of sediment entering the Min Jiang decreases by an order of magnitude. In contrast the fluvial driven processes (termed incision in our budget) are much more stable but significantly less important. Incision only accounts for 15% of the sediment deposited into the Min Jiang during the first decade after the earthquake. Fluvial erosion is only observed acting on sediment that has already been remobilised once, there is little evidence that the tributary channels can erode the landslide deposits directly. This further highlights the importance of hillslope processes in remobilising sediment prior to it being available for evacuation from the orogen. Fluvial erosion is likely slow at removing sediment from the tributary channel deposits due to the coarse nature of the stored sediment. Cobble and boulder sized grains are not uncommon and require significantly larger than average discharges to mobilise them. The coarse nature of the tributary channel deposits indicates that much of the sediment requires debris flows, large floods or in situ break down of the boulders before it can be mobilised out of the orogen.

It is important to point out that we have little to no constraints on the volume of sediment that leaves the tributary channel deposits unless it is by a catchment clearing debris flow. Without these constraints we have to assume that the volume of sediment that is entrained by our incision term is immediately removed from the tributary channel deposits. As most sediment will be deposited before it exits the tributary channel deposits it is possible our estimation of the sediment volume transported into the Min Jiang is an over estimation. Therefore we can be confident in stating that incision is a minor contributor to the sediment budget. Improving our estimation of the volume of sediment entering the Min Jiang via fluvial processes will require monitoring of both water and sediment discharge of the tributary catchments.

Finally, it is unlikely the incision mapped as part of the study is exclusively derived by fluvial processes. Debris flows are common on the tributary channel floors and these can mobilise sediment and create channels which may not separable from fluvially derived channels. It has also been suggested that debris flow activity in the tributary channel deposits could become more common through time as more aggradation occurs (Zhang and Zhang 2017; Fan et al. 2018). We observe a slight increase in the incision term in the final epochs of our sediment budget. If this increase is real and represents an increase in the volume of sediment entering the Min Jiang it is possible debris flow activity could contribute to this. If this increase in debris flow activity is an indicator of a potential increase in the frequency of large catchment clearing debris flows the tributary channel deposits could be evacuated rapidly during times of high sediment availability. However, without a clear understanding of the triggering mechanisms of the large catchment clearing debris flows it is not possible to determine a long-term rate by which sediment is exported from these deposits.

In August 2019 a large storm triggered 12 large catchment clearing debris flows in our study area, some in catchments where no debris flow had occurred for over 5 years (Fan et al. 2020; Yang et al. 2021). These events demonstrate the stochastic nature of the largest but most important events in mobilising sediment through the mountain range. Initial estimates of the volume of the debris flows suggests a total of 1.9×10^{-2} ($\pm3\times10^{-2}$) km^3 of sediment was transported by these events (Yang et al. 2021). However most of this volume was re-deposited within the tributary channel deposits. As a crude estimate of the volume of sediment deposited into the Min Jiang, we can extrapolate the recorded volume of a single debris flow fan over all of the 12 flows. The deposition fan of the Manianping catchment has an estimated volume of 7×10^{-4} km^3 (Yang et al. 2021) assuming all 12 flows were of equal magnitude, 8.4×10^{-3} km^3 of sediment was deposited into the Min Jiang. Including these flows into the final epoch of the step budget would increase the volume of sediment entering into the Min Jiang by an order of magnitude and return the sediment budget to magnitudes not seen since 2013. Interestingly many of the 2019 catchment clearing debris flows occurred without significant remobilisation of hillslope deposits, indicating they removed sediment only from the tributary channel deposits (Fan et al. 2020). If it is possible these flows could have evacuated over 20% of the sediment in the tributary channel deposits. These flows demonstrate the need for long-term (multi-decadal) observational records before predictions of future behaviour of post seismic landscapes can be made.

The Min Jiang drains into the Zipingpu reservoir a few kilometres after leaving the study area providing an excellent opportunity to identify whether the sediment dynamics discussed here can be identified downstream. A borehole of the centre of the reservoir drilled by Zhang et al. (2019) in 2016 identified that the earthquake had only had a slight impact on the sediment dynamics. No change in sedimentation rate was noticed, likely due to the distal location of the core relative to the Min Jiang entering the reservoir, but a change in the chemistry and grain size was observed (Zhang et al. 2019). Grain size increased, possibly indicating the transport of coarser coseismic landslide derived sediment, and the Rb/Sr ratio decreased potentially due to an influx of unweathered (fresh landslide derived) sediment into the reservoir. Crucially while these signals were recognised immediately after the earthquake the biggest response was observed after the 2010 debris flows where significant volumes of coseismically generated sediment was deposited into the rivers draining into the reservoir. This result agrees with our finding that debris flows are the major component in delivering sediment to the channel network. The borehole also suggests that the system is in a transport limited state as grain size and total runoff is well correlated indicating the need for large events to mobilise much of the sediment (Zhang et al. 2019).

Our and the results of others (West et al. 2014; Wang et al. 2017; Zhang and Zhang 2017; Zhang et al. 2019) indicate that much of the coseismically generated sediment is transport limited. It is either waiting on the hillslope to be remobilised by mass movements or in tributary channel deposits waiting for a flood or large debris flow. This could result in sediment residence times of 1000's of years which is likely to impact the long-term evolution of the landscape. Empirical and modelling studies suggest that the hillslope will continue to be perturbed for at least another decade before returning to background levels (Chen et al. 2020; Li et al. 2020; Shen et al. 2020; Yunus et al. 2020). As this trend in declining activity is driven by stabilisation rather than exhaustion it is likely the residence time of the coseismically generated sediment will be significantly longer. Large earthquakes such as the Wenchuan earthquake have a return period of 500 – 4000 years and if coseismically generated sediment can remain being reworked for similar timescales it is likely erosion rates will be altered (Li et al. 2017; Francis et al. 2020). The large volumes of sediment on the hillslopes, which are on average steeper than the likely friction angle of sediment, will continue to be mobilised, albeit much slower than immediately after the earthquake. Erosion rates in the tributary channels and the Min Jiang are likely to be lowered if the bedload is not mobilised at rates significant enough to abrade the bed. Deposits of landslide derived sediment have been linked to knickpoints within the Longmen Shan indicating the region is prone to long periods of reduced erosion (Ouimet et al. 2007; Fan et al. 2019a). If post seismic reduction of erosion rates is frequent and wide spread, it is possible that the largest earthquakes may have a positive impact on the long-term mass balance of the mountain range despite the huge amount of erosion they initiate.

6 Conclusions

Here we have quantified the sediment cascade of the 10 years following the 2008 Wenchuan earthquake. Using a multitemporal landslide inventory and constrained area – volume scaling relationships we tracked the evolution of 1.1 (±0.5) km^3 of sediment. Of this sediment just 3% was deposited into the Min Jiang, the major orogen draining river of the study area. 95% of the sediment deposited onto the hillslope during the earthquake remains there waiting to be mobilised into the channel network. The key process in mobilising coseismic sediment into the Min Jiang has been debris flows. The largest of these can deposit huge volumes of sediment from the tributary channels, overcoming the otherwise low transport capacity of the channels in these catchments. These large flows are highly stochastic and can occur after breaks of many years. Determining the frequency and magnitude of these events is crucial to estimating the residence time of the coseismically generated sediment. Finally, as large volumes of coseismically generated sediment can remain within the orogen for extended periods of time, their impact should be considered when modelling the long-term evolution of tectonically active mountain ranges.

Acknowledgments, Samples, and Data

The authors declare no known conflicts of interest.
This work was funded by the Newton Fund, Natural Environmental Research Council, Economic and Social Research Council, and National Science Foundation for China grant, NE/N012240/1,

the Funds for Creative Research Groups of China (Grant No. 41521002), and the Fund for International Cooperation (NSFC-RCUK_NERC), Resilience to Earthquake-induced landslide risk in China (grant No. 41661134010). The authors would like to thank the team of mappers who helped put together the mass movement inventory on which this study was based. We would also like to thank A. Densmore and M. Singer for useful discussions which greatly enhanced this paper.

The mass movement inventories upon which this study is based have been published (Fan et al, 2019) and can be found at https://doi.org/10.5281/zenodo.1405489.

References

Bennett, G.L. et al. 2014. A probabilistic sediment cascade model of sediment transfer in the Illgraben. *Water Resources Research* 50(2), pp. 1225–1244. Available at: http://doi.wiley.com/10.1002/2013WR013806.

Burchfiel, B.C. et al. 2008. A geological and geophysical context for the Wenchuan earthquake of 12 May 2008, Sichuan, People's Republic of China. *GSA Today* 18(7), pp. 4–11. doi: 10.1130/GSATG18A.1.

Campforts, B. et al. 2020. HyLands 1.0: A hybrid landscape evolution model to simulate the impact of landslides and landslide-derived sediment on landscape evolution. *Geoscientific Model Development* 13(9), pp. 3863–3886. doi: 10.5194/gmd-13-3863-2020.

Chang, D.S. et al. 2011. Field testing of erodibility of two landslide dams triggered by the 12 May Wenchuan earthquake. *Landslides* 8(October 2009), pp. 321–332. doi: 10.1007/s10346-011-0256-x.

Chen, H.X. et al. 2014. Evolution of debris flow properties and physical interactions in debris-flow mixtures in the Wenchuan earthquake zone. *Engineering Geology* 182(PB), pp. 136–147. Available at: http://dx.doi.org/10.1016/j.enggeo.2014.08.004.

Chen, M. et al. 2020. The long-term evolution of landslide activity near the epicentral area of the 2008 Wenchuan earthquake in China. *Geomorphology* 367, p. 107317. doi: 10.1016/j.geomorph.2020.107317.

Croissant, T. et al. 2019. Seismic cycles, earthquakes, landslides and sediment fluxes: Linking tectonics to surface processes using a reduced-complexity model. *Geomorphology* 339, pp. 87–103. doi: 10.1016/j.geomorph.2019.04.017.

Cui, P. et al. 2013. Scale amplification of natural debris flows caused by cascading landslide dam failures. *Geomorphology* 182(August 2010), pp. 173–189. doi: 10.1016/j.geomorph.2012.11.009.

Cui, P. et al. 2014. The mechanisms behind shallow failures in slopes comprised of landslide deposits. *Engineering Geology* 180, pp. 34–44. Available at: http://dx.doi.org/10.1016/j.enggeo.2014.04.009.

Dadson, S.J. et al. 2004. Earthquake-triggered increase in sediment delivery from an active mountain belt. *Geology* 32(8), p. 733. Available at: https://pubs.geoscienceworld.org/geology/article/32/8/733-736/29559.

Dahlquist, M.P. et al. 2018. Landslide-driven drainage divide migration. *Geology* 46(5), pp. 403–406. doi: https://doi.org/10.1130/G39916.1.

Dai, F.C. et al. 2011. Spatial distribution of landslides triggered by the 2008 Ms 8.0 Wenchuan earthquake, China. *Journal of Asian Earth Sciences* 40(4), pp. 883–895. doi: 10.1016/j.jseaes.2010.04.010.

Densmore, A.L. et al. 2007. Active tectonics of the Beichuan and Pengguan faults at the eastern margin of the Tibetan Plateau. *Tectonics* 26(4), pp. 1–17. doi: 10.1029/2006TC001987.

Densmore, A.L. et al. 2010. The role of late quaternary upper-crustal faults in the 12 may 2008 Wenchuan earthquake. *Bulletin of the Seismological Society of America* 100(5 B), pp. 2700–2712. doi: 10.1785/0120090294.

Densmore, A.L. et al. 2012. Reply to 'Isostasy can't be ignored'. *Nature Geoscience* 5(2), pp. 83–84. Available at: http://dx.doi.org/10.1038/ngeo1385.

Egholm, D.L. et al. 2013. Lifespan of mountain ranges scaled by feedbacks between landsliding and erosion by rivers. *Nature* 498(7455), pp. 475–478. doi: 10.1038/nature12218.

Fan, X. et al. 2018. Spatio-temporal evolution of mass wasting after the 2008 Mw 7 . 9 Wenchuan Earthquake revealed by a detailed multi-temporal inventory. *Landslides* 15(September), pp. 2325–2341. doi: 10.1007/s10346-018-1054-5.

Fan, X. et al. 2019a. Comment on 'Gigantic rockslides induced by fluvial incision in the Diexi area along the eastern margin of the Tibetan Plateau' by Zhao et al. (2019) Geomorphology 338, 27–42. *Geomorphology* (xxxx), p. 106963. Available at: https://doi.org/10.1016/j.geomorph.2019.106963.

Fan, X. et al. 2019b. Earthquake-Induced Chains of Geologic Hazards: Patterns, Mechanisms, and Impacts. *Reviews of Geophysics* . doi: 10.1029/2018RG000626.

Fan, X. et al. 2019c. Two multi-temporal datasets that track the enhanced landsliding after the 2008 Wenchuan earthquake. *Earth System Science Data* 11(1), pp. 35–55. Available at: https://www.earth-syst-sci-data.net/11/35/2019/.

Fan, X. et al. 2020. Rapidly evolving controls of landslides after a strong earthquake and implications for hazard assessments. *Geophysical Research Letters* 33(0), pp. 2–31. Available at: https://onlinelibrary.wiley.com/doi/10.1029/2020GL090509.

Francis, O.R. et al. 2020. The impact of earthquakes on orogen-scale exhumation. *Earth Surface Dynamics* 8(3), pp. 579–593. Available at: https://esurf.copernicus.org/articles/8/579/2020/.

Fusun, S. et al. 2013. Effects of different types of vegetation recovery on runoff and soil erosion on a Wenchuan earthquake-triggered landslide, China. *Journal of Soil and Water Conservation* 68(2), pp. 138–145. doi: 10.2489/jswc.68.2.138.

Gabet, E.J. and Mudd, S.M. 2006. The mobilization of debris flows from shallow landslides. *Geomorphology* 74(1–4), pp. 207–218. doi: 10.1016/j.geomorph.2005.08.013.

Gallen, S.F. et al. 2015. Coseismic landslides reveal near-surface rock strength in a highrelief, tectonically active setting. *Geology* 43(1), pp. 11–14. doi: 10.1130/G36080.1.

Godard, V. et al. 2010. Spatial distribution of denudation in Eastern Tibet and regressive erosion of plateau margins. *Tectonophysics* 491(1–4), pp. 253–274. Available at: http://dx.doi.org/10.1016/j.tecto.2009.10.026.

Guo, X. et al. 2016. Intensity-duration threshold of rainfall-triggered debris flows in the

Wenchuan Earthquake affected area, China. *Geomorphology* 253, pp. 208–216. doi: 10.1016/j.geomorph.2015.10.009.

Guzzetti, F. et al. 2009. Landslide volumes and landslide mobilization rates in Umbria, central Italy. *Earth and Planetary Science Letters* 279(3–4), pp. 222–229. Available at: http://dx.doi.org/10.1016/j.epsl.2009.01.005.

Hales, T.C. et al. 2009. Topographic and ecologic controls on root reinforcement. *Journal of Geophysical Research: Solid Earth* 114(3), pp. 1–17. doi: 10.1029/2008JF001168.

Hales, T.C. 2018. Modelling biome-scale root reinforcement and slope stability. *Earth Surface Processes and Landforms* 43(10), pp. 2157–2166. doi: 10.1002/esp.4381.

Hovius, N. et al. 2000. Supply and Removal of Sediment in a Landslide-Dominated Mountain Belt: Central Range, Taiwan. *The Journal of Geology* 108(1), pp. 73–89. Available at: http://www.journals.uchicago.edu/doi/10.1086/314387.

Hovius, N. et al. 2011. Prolonged seismically induced erosion and the mass balance of a large earthquake. *Earth and Planetary Science Letters* 304(3–4), pp. 347–355. Available at: http://dx.doi.org/10.1016/j.epsl.2011.02.005.

Hu, W. et al. 2016. Initiation processes for run-off generated debris flows in the Wenchuan earthquake area of China. *Geomorphology* 253, pp. 468–477. doi: 10.1016/j.geomorph.2015.10.024.

Hu, W. et al. 2017. Sensitivity of the initiation and runout of flowslides in loose granular deposits to the content of small particles: An insight from flume tests. *Engineering Geology* 231(July), pp. 34–44. Available at: https://doi.org/10.1016/j.enggeo.2017.10.001.

Huang, R. and Fan, X. 2013. The landslide story. *Nature Geoscience* 6(5), pp. 325–326. Available at: http://dx.doi.org/10.1038/ngeo1806.

Hubbard, J. and Shaw, J.H. 2009. Uplift of the Longmen Shan and Tibetan plateau, and the 2008 Wenchuan (M = 7.9) earthquake. *Nature* 458(7235), pp. 194–197. Available at: http://dx.doi.org/10.1038/nature07837.

Iverson, R.M. et al. 2000. Acute sensitivity of landslide rates to initial soil porosity. *Science* 290(5491), pp. 513–516. doi: 10.1126/science.290.5491.513.

Keefer, D.K. 2002. Investigating landslides caused by earthquakes - A historical review. *Surveys in Geophysics* 23(6), pp. 473–510. doi: 10.1023/A:1021274710840.

Kincey, M.E. et al. 2021. Evolution of coseismic and post-seismic landsliding after the 2015 M w 7.8 Gorkha earthquake, Nepal. *Journal of Geophysical Research: Earth Surface* . doi: 10.1029/2020jf005803.

Kirby, E. and Ouimet, W. 2011. Tectonic geomorphology along the eastern margin of Tibet: insights into the pattern and processes of active deformation adjacent to the Sichuan Basin. *Geological Society, London, Special Publications* 353(1), pp. 165–188. Available at: http://sp.lyellcollection.org/lookup/doi/10.1144/SP353.9.

Koi, T. et al. 2008. Prolonged impact of earthquake-induced landslides on sediment yield in a mountain watershed: The Tanzawa region, Japan. *Geomorphology* 101(4), pp. 692–702. doi: 10.1016/j.geomorph.2008.03.007.

Korup, O. 2012. Earth's portfolio of extreme sediment transport events. *Earth-Science Reviews* 112(3–4), pp. 115–125. Available at: http://dx.doi.org/10.1016/j.earscirev.2012.02.006.

Larsen, I.J. et al. 2010. Landslide erosion controlled by hillslope material. *Nature Geoscience* 3(4), pp. 247–251. Available at: http://dx.doi.org/10.1038/ngeo776.

Li, C. et al. 2020. Landscape evolution of the Wenchuan earthquake-stricken area in response to future climate change. *Journal of Hydrology* 590, p. 125244. Available at: https://doi.org/10.1016/j.jhydrol.2020.125244.

Li, G. et al. 2014. Seismic mountain building: Landslides associated with the 2008 Wenchuan earthquake in the context of a generalized model for earthquake volume balance. *Geochemistry, Geophysics, Geosystems* 15(4), pp. 833–844. Available at: http://doi.wiley.com/10.1002/2013GC005067.

Li, G. et al. 2016. Connectivity of earthquake-triggered landslides with the fluvial network: Implications for landslide sediment transport after the 2008 Wenchuan earthquake. *Journal of Geophysical Research: Earth Surface* 121(4), pp. 703–724. Available at: http://doi.wiley.com/10.1002/2015JF003718.

Li, G. et al. 2017. Earthquakes drive focused denudation along a tectonically active mountain front. *Earth and Planetary Science Letters* 472, pp. 253–265. Available at: http://dx.doi.org/10.1016/j.epsl.2017.04.040.

Lin, G.-W. et al. 2008. Effects of earthquake and cyclone sequencing on landsliding and fluvial sediment transfer in a mountain catchment. *Earth Surface Processes and Landforms* 33(9), pp. 1354–1373. Available at: http://doi.wiley.com/10.1002/esp.1716.

Liu-Zeng, J. et al. 2009. Co-seismic ruptures of the 12 May 2008, Ms8.0 Wenchuan earthquake, Sichuan: East-west crustal shortening on oblique, parallel thrusts along the eastern edge of Tibet. *Earth and Planetary Science Letters* 286(3–4), pp. 355–370. Available at: http://dx.doi.org/10.1016/j.epsl.2009.07.017.

Malamud, B.D. et al. 2004. Landslides, earthquakes, and erosion. *Earth and Planetary Science Letters* 229(1–2), pp. 45–59. doi: 10.1016/j.epsl.2004.10.018.

Marc, O. et al. 2015. Transient changes of landslide rates after earthquakes. *Geology* 43(10), pp. 883–886. doi: 10.1130/G36961.1.

Marc, O. et al. 2016a. A seismologically consistent expression for the total area and volume of earthquake-triggered landsliding. *Journal of Geophysical Research: Earth Surface* 121(4), pp. 640–663. Available at: http://doi.wiley.com/10.1002/2015JF003732.

Marc, O. et al. 2016b. The mass balance of earthquakes and earthquake sequences. *Geophysical Research Letters* 43(8), pp. 3708–3716. doi: 10.1002/2016GL068333.

Marc, O. and Hovius, N. 2015. Amalgamation in landslide maps: Effects and automatic detection. *Natural Hazards and Earth System Sciences* 15(4), pp. 723–733. doi: 10.5194/nhess-15-723-2015.

McGuire, L.A. et al. 2016. Constraining the relative importance of raindrop- and flow-driven sediment transport mechanisms in postwildfire environments and implications for recovery time scales. *Journal of Geophysical Research: Earth Surface* 121(11), pp. 2211–2237. doi: 10.1002/2016JF003867.

Mudd, S.M. et al. 2020. LSDtopotools/LSDTopoTools2: LSDTopoTools2 v0.3. Available at: https://doi.org/10.5281/zenodo.3769703#.X6AA9d3MMXY.mendeley [Accessed: 2 November 2020].

Ouimet, W.B. et al. 2007. The influence of large landslides on river incision in a transient landscape: Eastern margin of the Tibetan Plateau (Sichuan, China). *Bulletin of the Geological Society of America* 119(11–12), pp. 1462–1476. doi: 10.1130/B26136.1.

Ouimet, W.B. et al. 2009. Beyond threshold hillslopes: Channel adjustment to base-level fall in tectonically active mountain ranges. *Geology* 37(7), pp. 579–582. doi: 10.1130/G30013A.1.

Pain, C.F. and Bowler, J.M. 1973. Denudation following the November 1970 earthquake. *Zeitschrift Fur Geomorphologie* 18, pp. 92–104.

Parker, R.N. et al. 2011. Mass wasting triggered by the 2008 Wenchuan earthquake is greater than orogenic growth. *Nature Geoscience* 4(7), pp. 449–452. Available at: http://dx.doi.org/10.1038/ngeo1154.

Pearce, A.J. and Watson, A.J. 1986. Effects of earthquake-induced landslides on sediment budget and transport over a 50-yr period. *Geology* 14, pp. 52–55.

Roback, K. et al. 2018. The size, distribution, and mobility of landslides caused by the 2015 Mw7.8 Gorkha earthquake, Nepal. *Geomorphology* 301, pp. 121–138. Available at: https://doi.org/10.1016/j.geomorph.2017.01.030.

Royden, L.H. et al. 2008. The Geological Evolution of the Tibetan Plateau. *Science* 321(5892), pp. 1054–1058. Available at: https://www.sciencemag.org/lookup/doi/10.1126/science.1155371.

Schmidt, K.M. and Montgomery, D.R. 1995. Limits to Relief. *Science* 270(5236), pp. 617–620. Available at: http://www.sciencemag.org/cgi/doi/10.1126/science.270.5236.617.

Schwanghart, W. et al. 2016. Repeated catastrophic valley infill following medieval earthquakes in the Nepal Himalaya. *Science* 351(6269), pp. 147–150. doi: 10.1126/science.aac9865.

Shen, P. et al. 2020. Declining geohazard activity with vegetation recovery during first ten years after the 2008 Wenchuan earthquake. *Geomorphology* 352, p. 106989. Available at: https://doi.org/10.1016/j.geomorph.2019.106989.

Stolle, A. et al. 2017. Catastrophic valley fills record large Himalayan earthquakes, Pokhara, Nepal. *Quaternary Science Reviews* 177, pp. 88–103. Available at: https://doi.org/10.1016/j.quascirev.2017.10.015.

Stolle, A. et al. 2019. Protracted river response to medieval earthquakes. *Earth Surface Processes and Landforms* 44(1), pp. 331–341. Available at: http://doi.wiley.com/10.1002/esp.4517.

Tang, C. et al. 2012. Catastrophic debris flows on 13 August 2010 in the Qingping area, southwestern China: The combined effects of a strong earthquake and subsequent rainstorms. *Geomorphology* 139–140(August 2010), pp. 559–576. Available at: http://dx.doi.org/10.1016/j.geomorph.2011.12.021.

Tang, C. et al. 2016. Analysing post-earthquake landslide activity using multi-temporal landslide inventories near the epicentral area of the 2008 Wenchuan earthquake. *Natural Hazards and Earth System Sciences* 16(12), pp. 2641–2655. doi: 10.5194/nhess-16-2641-2016.

Tolorza, V. et al. 2019. Suspended Sediments in Chilean Rivers Reveal Low Postseismic Erosion After the Maule Earthquake (Mw 8.8) During a Severe Drought. *Journal of Geophysical Research: Earth Surface* 124(6), pp. 1378–1397. Available at: https://onlinelibrary.wiley.com/doi/abs/10.1029/2018JF004766.

Turowski, J.M. and Rickenmann, D. 2009. Tools and cover effects in bedload transport observations in the Pitzbach, Austria. *Earth Surface Processes and Landforms* 34(1), pp. 26–37. Available at: http://doi.wiley.com/10.1002/esp.1686.

Vanmaercke, M. et al. 2014. Seismic controls on contemporary sediment export in the Siret river catchment, Romania. *Geomorphology* 216, pp. 247–262. Available at: http://dx.doi.org/10.1016/j.geomorph.2014.04.008.

Vanmaercke, M. et al. 2017. Exploring the effects of seismicity on landslides and catchment sediment yield: An Italian case study. *Geomorphology* 278, pp. 171–183. Available at: http://dx.doi.org/10.1016/j.geomorph.2016.11.010.

Wang, J. et al. 2015. Controls on fluvial evacuation of sediment from earthquake-triggered landslides. *Geology* 43(2), pp. 115–118. doi: 10.1130/G36157.1.

Wang, J.J. et al. 2013. Angle of repose of landslide debris deposits induced by 2008 Sichuan Earthquake. *Engineering Geology* 156, pp. 103–110. Available at: http://dx.doi.org/10.1016/j.enggeo.2013.01.021.

Wang, W. et al. 2017. Perturbation of fluvial sediment fluxes following the 2008 Wenchuan earthquake. *Earth Surface Processes and Landforms* 42(15), pp. 2611–2622. doi: 10.1002/esp.4210.

West, A.J. et al. 2014. Dilution of10Be in detrital quartz by earthquake-induced landslides: Implications for determining denudation rates and potential to provide insights into landslide sediment dynamics. *Earth and Planetary Science Letters* 396, pp. 143–153. Available at: http://dx.doi.org/10.1016/j.epsl.2014.03.058.

Wilkinson, P.L. et al. 2002. An integrated hydrological model for rain-induced landslide prediction. *Earth Surface Processes and Landforms* 27(12), pp. 1285–1297. doi: 10.1002/esp.409.

Williams, J.G. et al. 2018. Satellite-based emergency mapping using optical imagery: Experience and reflections from the 2015 Nepal earthquakes. *Natural Hazards and Earth System Sciences* 18(1), pp. 185–205. doi: 10.5194/nhess-18-185-2018.

Yang, F. et al. 2021. Catastrophic debris flows triggered by the 20 August 2019 rainfall, a decade since the Wenchuan earthquake, China. *Landslides* (October 2020). doi: 10.1007/s10346-021-01713-6.

Yanites, B.J. et al. 2010. How rivers react to large earthquakes: Evidence from central Taiwan. *Geology* 38(7), pp. 639–642. Available at: http://pubs.geoscienceworld.org/geology/article/38/7/639/130315/How-rivers-react-to-large-earthquakes-Evidence.

Yunus, A.P. et al. 2020. Decadal vegetation succession from MODIS reveals the spatio-temporal evolution of post-seismic landsliding after the 2008 Wenchuan earthquake. *Remote Sensing of Environment* 236(October 2019), p. 111476. Available at:

https://doi.org/10.1016/j.rse.2019.111476.

Zhang, F. et al. 2019. Monsoonal control on a delayed response of sedimentation to the 2008 Wenchuan earthquake. *Science Advances* 5(6). Available at: http://advances.sciencemag.org/lookup/doi/10.1126/sciadv.aav7110.

Zhang, S. et al. 2014. Relationships among three repeated large-scale debris flows at Pubugou Ravine in the Wenchuan earthquake zone. *Canadian Geotechnical Journal* 51(9), pp. 951–965. Available at: http://www.nrcresearchpress.com/doi/abs/10.1139/cgj-2013-0368.

Zhang, S. and Zhang, L.M. 2017. Impact of the 2008 Wenchuan earthquake in China on subsequent long-term debris flow activities in the epicentral area. *Geomorphology* 276, pp. 86–103. Available at: http://dx.doi.org/10.1016/j.geomorph.2016.10.009.

[Earth Surface]

Supporting Information for

[The Fate of Sediment After a Large Earthquake]

[Oliver Francis[1,2,*], Xuanmei Fan[3], Tristram Hales[1,2], Daniel Hobley[2], Qiang Xu[3], Runqiu Huang[3]]

[[1]Sustainable Places Research Institute, Cardiff University, Cardiff, United Kingdom

[2]School of Earth and Environmental Sciences, Cardiff University, Cardiff, United Kingdom

[3]State Key Laboratory for Geohazard Prevention and Geoenvironment Protection, Chengdu University of Technology, Chengdu, China

Corresponding author: Oliver Francis (Oliver.Francis@gfz-potsdam.de)

*Now at Section 4.7: Earth Surface Process Modelling, German Research Centre for Geosciences (GFZ), Potsdam, Germany]

Contents of this file

Introduction

This file including the supporting information for The Fate of Sediment After a Large Earthquake. These support and provide further details of the methods and results described within the main text of the manuscript.

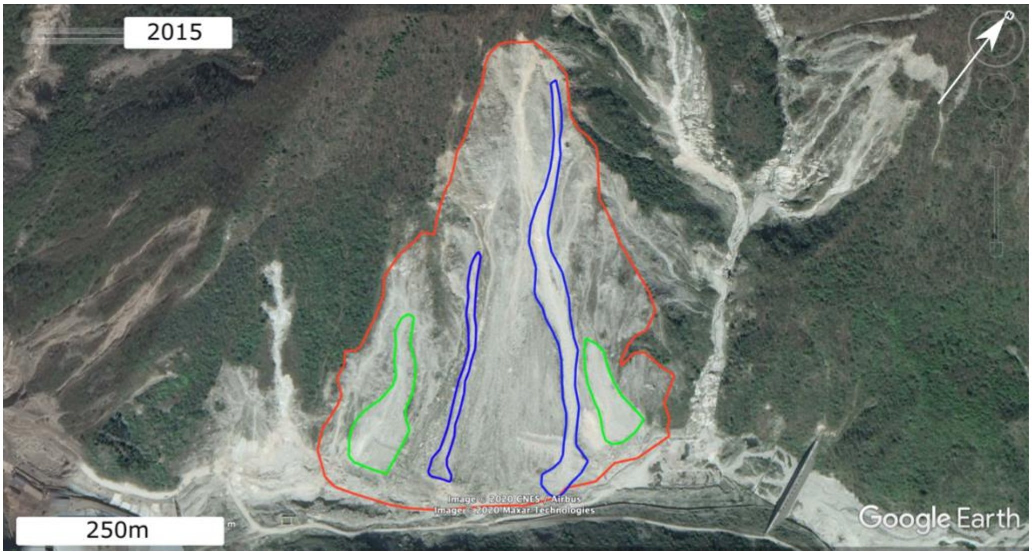

Figure S1: A subsection of a mapped catchment with examples of key mass movement types highlighted in different colours. A coseismic landslide is mapped with a red online and we can see it has been remobilised several times since the earthquake. Unchannelised remobilisations are outlined in green while channelized remobilisations are mapped in blue. Debris flows are mapped based upon the same criteria as channelised remobilisation.

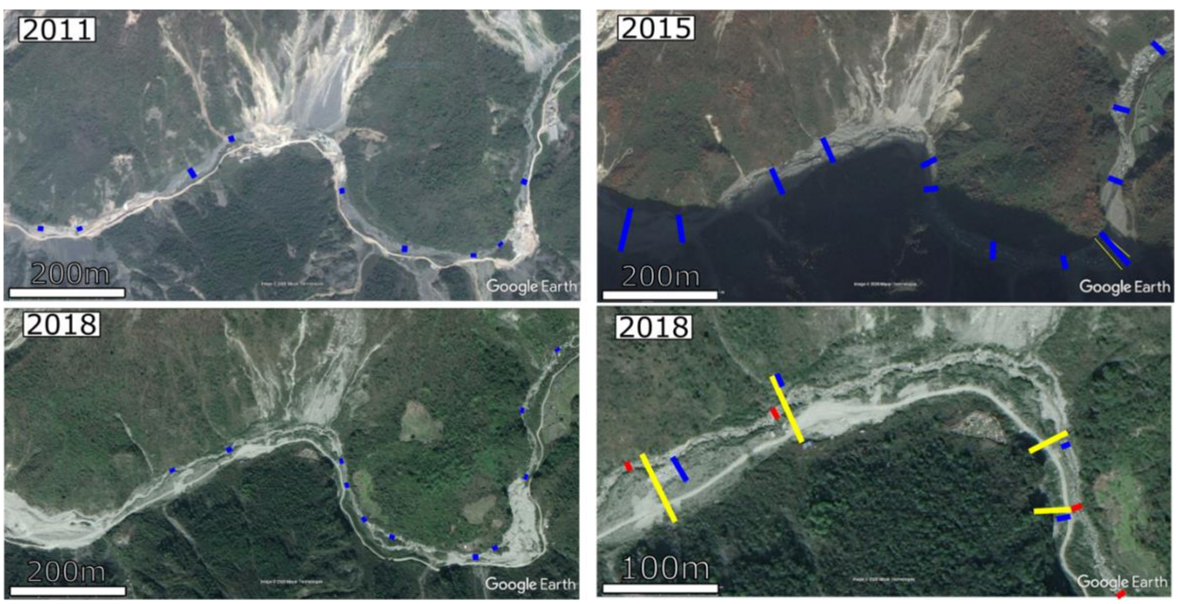

Figure S2: Examples of the mapping of tributary channel deposit cross sections. The first 3 images are of the same area through time. For each image the channel deposit is mapped to the edge of the visible sediment at regular intervals, shown in blue. The final image shows a subsection of a catchment with the mapped cross sections in different colours. The cross section from 2011 is mapped in blue, 2011 in yellow and 2018 in red. Due to rectification errors within Google Earth the cross sections are not in the exact same position, however care was taken to ensure repeat surveys were taken as close as possible.

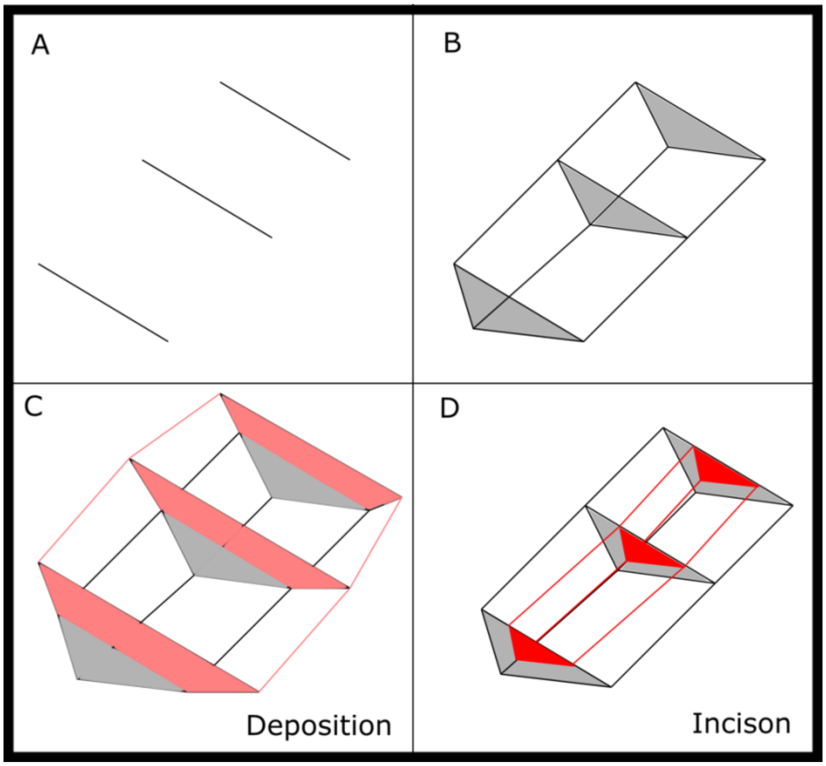

Figure S3: A cartoon illustrating the estimation of channel deposit volumes from the mapped cross sections. A) the cross sections are drawn. B) the along channel distance between the cross section is calculated and a triangular cross section is assumed. Multiplying the distance by the area provides an estimate for the volume contained in the tributary channel deposits. C) The cross sections are remapped and the widths have increased. To determine the volume of sediment deposited the triangular cross section and volume is recalculated with the new width and the previous volume is removed. D) if the width has stabilised, we assume no deposition has occurred. Therefore, we map the width of the actively incising channel and estimate the volume of sediment removed by the channel by again assuming a triangular cross section.

Date of image	Source of Image	Resolution	Coverage
May – July 2008	Aerial photography	1 – 2.5m	97%
April 2011	Aerial photography and Worldview satellite	0.5 – 1m	99%
April 2013	Aerial photography and Pleiades satellite	0.5 - 2m	95%
April 2015	Spot 6 satellite	1.5m	99%
April 2017	Spot 6 satellite	3m	93%
April 2018	Spot 6 satellite	3m	93%

Table S1. The date, source and resolution of the images used in the development of the inventory. Coverage describes the percentage of the study area covered by the imagery at each time step.

Parameter set	Median volume (km^3)	Minimum volume (km^3)	Maximum volume (km^3)
Table 1	0.27	0.14	0.38
Average depths of 1, 2 or 3 meters	7.3	1.5	157
Average depth between 0.05 and 0.95 meters and shallow soil landslides (Larsen)	4×10^{-2}	1.8×10^{-2}	0.15
Estimated increase in tributary channel deposits	-	2.12×10^{-2}	4.9×10^{-2}

Table S2. The estimated volume entering the tributary channel deposits using different combinations of area-volume scaling relationships. The final row contains the estimated volume of the channel deposits from the analysis of the cross sections. Any scaling relationships which produce an estimate of volumes substantially different from the independent estimate of tributary channel deposits is discounted.